


# Transmittance contrast-induced photocurrent: A general strategy for self-powered photodetectors based on MXene electrodes

Hailong Ma<sup>1</sup> | Huajing Fang<sup>1</sup>  | Jiaqi Li<sup>1</sup> | Ziqing Li<sup>2</sup>  |  
Xiaosheng Fang<sup>2</sup>  | Hong Wang<sup>3</sup> 

<sup>1</sup>Center for Advancing Materials Performance from the Nanoscale (CAMP-Nano), State Key Laboratory for Mechanical Behavior of Materials, Xi'an Jiaotong University, Xi'an, the People's Republic of China

<sup>2</sup>Department of Materials Science, Institute of Optoelectronics, Fudan University, Shanghai, the People's Republic of China

<sup>3</sup>Department of Materials Science and Engineering & Shenzhen Engineering Research Center for Novel Electronic Information Materials and Devices, Southern University of Science and Technology, Shenzhen, the People's Republic of China

## Correspondence

Huajing Fang, Center for Advancing Materials Performance from the Nanoscale (CAMP-Nano), State Key Laboratory for Mechanical Behavior of Materials, Xi'an Jiaotong University, Xi'an 710049, the People's Republic of China.  
Email: fanghj@xjtu.edu.cn

Xiaosheng Fang, Department of Materials Science, Institute of Optoelectronics, Fudan University, Shanghai 200433, the People's Republic of China.  
Email: xshfang@fudan.edu.cn

Hong Wang, Department of Materials Science and Engineering & Shenzhen Engineering Research Center for Novel Electronic Information Materials and Devices, Southern University of Science and Technology, Shenzhen 518055, the People's Republic of China.  
Email: wangh6@sustech.edu.cn

## Funding information

National Natural Science Foundation of China, Grant/Award Number: 51902250; Guangdong Provincial Key Laboratory Program, Grant/Award Number: 2021B1212040001; Shenzhen Science and Technology Program, Grant/Award Number: KQTD20180411143514543; Shenzhen DRC project, Grant/Award Number: [2018]1433

## Abstract

The regulation of carrier generation and transport by Schottky junctions enables effective optoelectronic conversion in optoelectronic devices. A simple and general strategy to spontaneously generate photocurrent is of great significance for self-powered photodetectors but is still being pursued. Here, we propose that a photocurrent can be induced at zero bias by the transmittance contrast of MXene electrodes in MXene/semiconductor Schottky junctions. Two MXene electrodes with a large transmittance contrast (84%) between the thin and thick zones were deposited on the surface of a semiconductor wafer using a simple and robust solution route. Kelvin probe force microscopy tests indicated that the photocurrent at zero bias could be attributed to asymmetric carrier generation and transport between the two Schottky junctions under illumination. As a demonstration, the MXene/GaN ultraviolet (UV) photodetector exhibits excellent performance superior to its counterpart without transmittance contrast, including high responsivity (81 mA W<sup>-1</sup>), fast response speed (less than 31 and 29 ms) and ultrahigh on/off ratio (1.33 × 10<sup>6</sup>), and good UV imaging capability. Furthermore, this strategy has proven to be universal for first- to third-generation semiconductors such as Si and GaAs. These results provide a facile and cost-effective route for high-performance self-powered photodetectors and demonstrate the versatile and promising applications of MXene electrodes in optoelectronics.

## KEYWORDS

GaN, MXene, Schottky junction, self-powered photodetector, transmittance contrast

This is an open access article under the terms of the [Creative Commons Attribution](https://creativecommons.org/licenses/by/4.0/) License, which permits use, distribution and reproduction in any medium, provided the original work is properly cited.

© 2024 The Authors. *InfoMat* published by UESTC and John Wiley & Sons Australia, Ltd.

## 1 | INTRODUCTION

Photodetectors, a type of sensor that can convert optical signals into electrical signals, underpin modern applications such as environmental sensing, medical imaging, optical communication, and machine vision.<sup>1–3</sup> Up to now, most photodetectors in actual use require additional power sources to separate and collect photogenerated electrons and holes to obtain considerable responsivity, which not only increases the complexity and cost of the device, but also restricts their applications in some fields such as wireless sensor networks and in-situ medical therapy monitoring.<sup>4–6</sup> With the development of emerging technologies, such as the Internet of Things and wearable electronics, self-powered photodetectors that can operate without an external power source are highly desired because of their ultra-low dark current, high integrability, and low power consumption.<sup>7–9</sup> Since the conversion of light into electrical signals is inseparable from both semiconductors and metal electrodes, Schottky junctions at the metal/semiconductor interface are widely used in various optoelectronic devices. The built-in electric field at the Schottky junction interface enables spontaneous separation and directional transport of photogenerated carriers at zero bias. Hence, constructing Schottky junctions is an effective way to implement self-powered photodetectors and has attracted much attention in recent years.<sup>10–12</sup> However, all of these need to be achieved by employing two different electrode materials or electrode contact areas, which is not only a cumbersome process, but also their performance is not very high due to poor electrode contact and undesired Fermi level pinning.<sup>8,13–15</sup> A simple and general strategy for constructing high-performance self-powered photodetectors based on Schottky junctions is still urgently required.

The rise in two-dimensional (2D) materials has injected fresh blood into the semiconductor and optoelectronics industries.<sup>16,17</sup> Because the van der Waals heterojunctions greatly enrich the interface design flexibility in optoelectronics, 2D materials, such as graphene and transition metal dichalcogenides (TMD), have already set off a technological revolution in photodetectors.<sup>18,19</sup> Among the various 2D materials, transition metal carbides and nitrides (MXenes) demonstrate many fascinating applications in electronics and optoelectronics owing to their extraordinary electrical and optical properties.<sup>20–23</sup> As a representative of MXenes,  $\text{Ti}_3\text{C}_2\text{T}_x$  (where T stands for the surface terminations such as  $-\text{O}$ ,  $-\text{OH}$ , and  $-\text{F}$ ) shows excellent characteristics such as high electronic conductivity, adjustable work function, and transparency and solution processability, inspiring researchers to develop it as a building block for

photodetectors.<sup>24–26</sup> For example, Gao et al. fabricated a self-powered photodetector based on a MXene/Si/Ti-Au vertical Schottky junction by drop-casting  $\text{Ti}_3\text{C}_2\text{T}_x$  colloidal solutions of different concentrations on the surface of a silicon wafer, and investigated the influence of colloidal solution concentration on the conductivity and transmittance of the  $\text{Ti}_3\text{C}_2\text{T}_x$  electrode and the device performance.<sup>27</sup> Yang et al. demonstrated a large-area and flexible photodetector array spray-coated on common paper. A remarkable on/off ratio of 2300 and fast speed of 18 ms were achieved owing to the well-matched Schottky junction between the 2D  $\text{CsPbBr}_3$  and  $\text{Ti}_3\text{C}_2\text{T}_x$  nanosheets.<sup>28</sup> Our group designed a transparent ultraviolet (UV) photodetector with ultrahigh responsivity based on MXene/ $\text{TiO}_2$  Schottky junctions, where MXene was used to induce a photogating effect to improve the separation of photogenerated carriers.<sup>29</sup> Photodetectors based on Schottky junctions formed by MXene with other materials such as GaN thin film, InSe nanosheet, and PbS quantum dot have also been investigated.<sup>30–32</sup> Despite the exciting progress, a general device configuration based on all-MXene electrodes for self-powered photodetectors has not yet been proposed.

Looking at the basic physical process of self-powered photodetection based on Schottky junctions, physical or electronic asymmetric structures, such as asymmetric electrode work functions or electrode contact areas, are the key to generating a photocurrent at zero bias.<sup>14,15,33–35</sup> Some researches have demonstrated that the Schottky junction can also be regulated by illumination, which inspired us to implement self-powered photodetectors via asymmetric illumination.<sup>36–39</sup> In this work, we propose a general strategy for constructing self-powered photodetectors based on MXene electrodes with transmittance contrast. By depositing MXene films with different transmittance on the semiconductor surface, an appreciable photocurrent can be induced under illumination because of the asymmetric carrier generation and transport between two Schottky junctions with different electrode transmittances. Devices without transmittance contrast of MXene electrodes are much inferior, regardless of the point or surface light source. Such a general strategy can be easily realized by an all-solution processing approach, getting rid of expensive deposition equipments and harsh vacuum environmental requirements. The demonstration case with the MXene/GaN self-powered photodetector shows an outstanding overall performance with high responsivity ( $81 \text{ mA W}^{-1}$ ), fast response speed (less than 31 and 29 ms) and ultrahigh on/off ratio ( $1.33 \times 10^6$ ), enabling it to perform well as a single sensing pixel in a UV imaging system. Finally, we proved the universal applicability of this strategy by extending the MXene/semiconductor interface to different materials and obtained

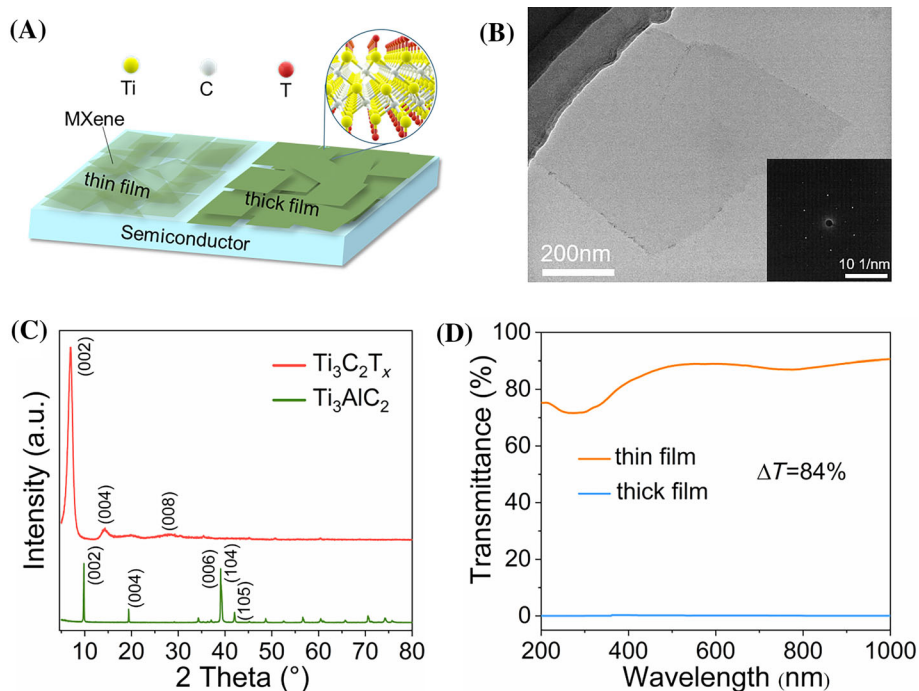


**FIGURE 1** (A) Schematic of the general device structure with MXene electrodes. (B) TEM image of the prepared  $\text{Ti}_3\text{C}_2\text{T}_x$  nanosheets and inset shows the SAED pattern. (C) XRD patterns of  $\text{Ti}_3\text{AlC}_2$  and  $\text{Ti}_3\text{C}_2\text{T}_x$ . (D) Transmittance spectra of spin-coated and drop-casted MXene films.

considerable performance in MXene/Si and MXene/GaAs photodetectors with similar configurations.

## 2 | RESULTS AND DISCUSSION

Figure 1A shows a schematic of the general device structure, in which MXene films with different thicknesses prepared by spin-coating and drop-coating were used as electrodes on the semiconductor surface with a spacing of 1 mm. The specific fabrication process is shown in Figure S1. Details regarding MXene colloid synthesis and device fabrication can be found in the Section 4. Figure 1B shows a transmission electron microscope (TEM) image of the prepared  $\text{Ti}_3\text{C}_2\text{T}_x$  nanosheets. Ultrathin nanosheet with a lateral size exceeding  $1\ \mu\text{m}$  confirms the successful delamination of  $\text{Ti}_3\text{C}_2\text{T}_x$  through lithium ions intercalation and ultrasonic bath. The selected area electron diffraction (SAED) pattern in the inset shows a typical hexagonal symmetric diffraction pattern, indicating good crystallinity of the prepared MXene nanosheets. The atomic force microscopy (AFM) image in Figure S2 shows the height profile of the MXene nanosheets, from which the thickness of the nanosheets was measured about 1.5 nm, corresponding to a single layer of MXene.<sup>40</sup> The quality of the prepared MXene was further evaluated by Raman spectroscopy and x-ray

photoelectron spectroscopy (XPS) tests, and the results are shown and discussed in detail in Figures S3 and S4. Figure 1C shows the x-ray diffraction (XRD) patterns of the  $\text{Ti}_3\text{AlC}_2$  MAX phase and as-prepared  $\text{Ti}_3\text{C}_2\text{T}_x$  film. After etching and delamination, almost all the high-angle peaks of  $\text{Ti}_3\text{AlC}_2$  disappeared and the (002) peak shifted from  $9.8^\circ$  to  $6.9^\circ$ , implying the successful removal of Al atoms from  $\text{Ti}_3\text{AlC}_2$  and the exfoliation of the MXene nanosheets.<sup>41,42</sup> The high intensity of the (002) peak indicates the high c-oriented stacking of the deposited MXene film.<sup>43</sup> Figure 1D shows the transmittance spectra of MXene films prepared by spin coating and drop casting. The average transmittance of the spin-coated MXene film is higher than 80% in the wavelength range of 200–1000 nm, whereas that of the drop-casted MXene film is almost zero, resulting in an average transmittance contrast of approximately 84% between two MXene films. The significant transmittance contrast is derived from the thickness difference of approximately 90 nm (see Figure S5) between them. The scanning electron microscope (SEM) images in Figure S6 show the surface morphologies of different MXene films. Both have a similar complete film structure formed by the overlapping and interconnecting MXene nanosheets, which ensures their good electrical conductivity. The thickness of the MXene thin and thick films measured by ellipsometry are 44 and 126 nm, respectively (see Figure S7).

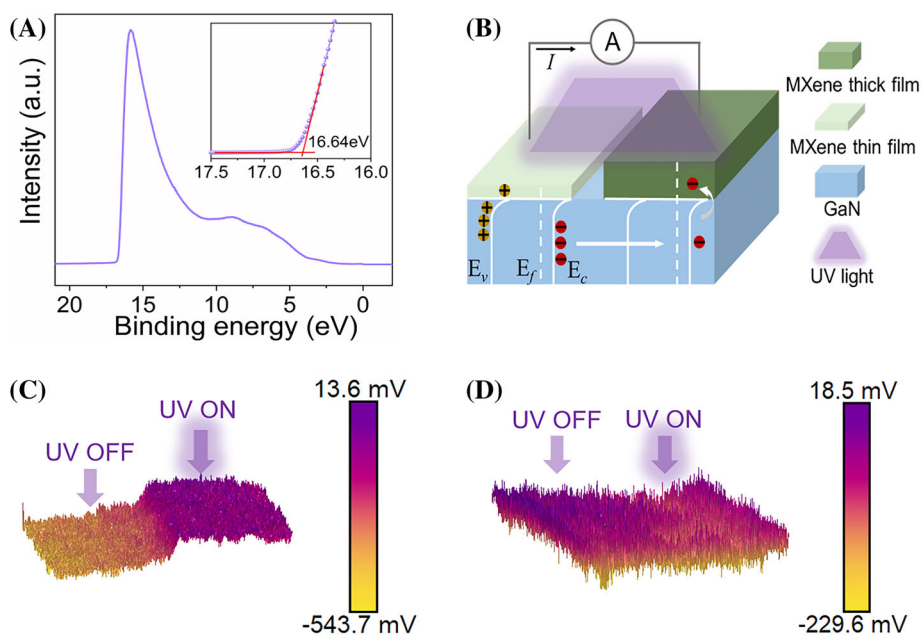


**FIGURE 2** (A) UPS spectrum of MXene thin film. (B) Schematic diagram of the band structure and carrier transfer process at the MXene/GaN Schottky junctions under UV illumination. The surface electrostatic potentials of (C) the MXene thin film and (D) thick film on the GaN surface before and after UV illumination.

Theoretically, the designed device prototype is feasible for any Schottky contacted MXene/semiconductor structures. For simplicity, GaN, a typical third-generation semiconductor, was selected as an example in our detailed discussion. Then, this strategy was proved to be also applicable to the first- and second-generation semiconductors. First, the work function of the prepared MXenes was measured using ultraviolet photoelectron spectroscopy (UPS) spectrum. As shown in Figure 2A, the work function of MXene thin film is calculated as 4.58 eV by subtracting the secondary electron cut-off energy (16.64 eV) from the incident ultraviolet photon energy (21.22 eV), which is similar to the previously reported value of 4.56 eV.<sup>11</sup> The reported work function of GaN is approximately 4 eV,<sup>30,44</sup> which is significantly smaller than that of MXene. Therefore, a Schottky junction can be formed between MXene and GaN. The work function calculated from the UPS spectrum of the MXene thick film is 4.54 eV (Figure S8), which is very close to that of the MXene thin film, indicating that the thickness has no effect on the work function of the MXene film. Figure 2B shows the specific mechanism of the photocurrent induced by transmittance contrast. When MXene is deposited on the GaN surface, electrons tunnel from GaN to MXene owing to its lower Fermi level, leaving an equal number of holes in GaN. In the equilibrium state, the Fermi levels of GaN and MXene tend to be the same ( $E_f$ ), and a depletion region is formed in the GaN near the interface due to the depletion of electrons, which causes

the GaN conduction band ( $E_c$ ) to bend upward towards MXene, forming a Schottky barrier. A built-in electric field exists from GaN to MXene in the depletion region. For the Schottky junction with a highly transparent MXene thin film, a large number of photogenerated electron-hole pairs can be generated in the GaN under UV illumination. Then, the photogenerated electrons drift into the bulk GaN, while the holes drift to the MXene thin film driven by the built-in electric field. In contrast, there is no generation of photocarriers in GaN under the MXene thick film because of the nearly zero UV transmittance of the MXene thick film. As a result, the electrons diffuse laterally in the GaN driven by the concentration difference and overcome the Schottky barrier to be injected into the MXene thick film, and finally recombine with the holes in the MXene thin film through the external circuit, forming a photocurrent ( $I_{ph}$ ). To verify the proposed carrier transfer mechanism, the changes in the surface electrostatic potential of different MXene films on GaN before and after UV illumination were measured by Kelvin probe force microscopy (KPFM). As shown in Figure 2C, the surface potential of the MXene thin film on GaN increased significantly after UV illumination, implying that the photogenerated holes were injected from GaN into the MXene thin film. In contrast, the surface potential of MXene thick film did not change noticeably after UV illumination because of the absence of photogenerated carrier injection (Figure 2D). KPFM tests confirmed the asymmetric carrier generation and

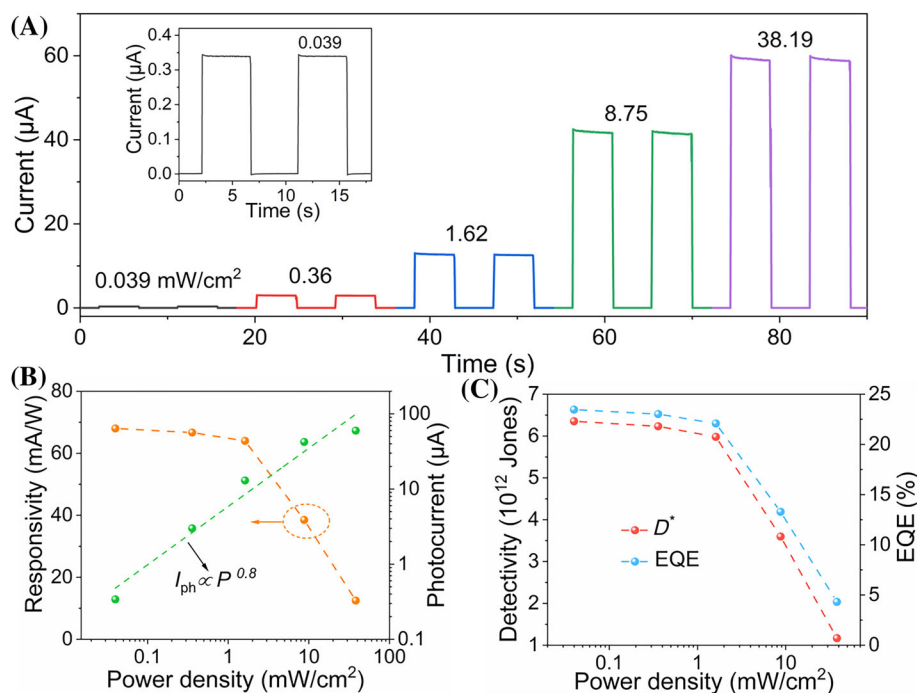


**FIGURE 3** (A) Photoswitching behaviors of the MXene/GaN photodetector under different light power density at 0 V. (B) Photocurrent and responsivity under different light power density at 360 nm. (C)  $D^*$  and EQE under different light power density at 360 nm.

injection resulting from the transmittance contrast of the MXene electrodes.

Next, we comprehensively investigated the performance of MXene/GaN as a self-powered UV photodetector. The temporal photoresponse of the device at zero bias was first measured using a 360 nm laser with adjustable light power. As shown in Figure 3A, the photodetector can be reversibly switched between on and off state, and the photocurrent (current difference between light and dark state,  $I_{ph} = I_{light} - I_{dark}$ ) increases gradually from 397 nA to 60 μA with increasing light power density from 0.039 to 38.19 mW cm<sup>-2</sup>. Derived from large photocurrent and extremely low dark current of 45 pA at 0 V (Figure S9), the photodetector exhibits an ultrahigh on/off ratio ( $I_{light}/I_{dark}$ ) of  $1.33 \times 10^6$ . The quantitative relationship between photocurrent and light power density can be fitted using the following power law:

$$I_{ph} \propto P^\alpha \quad (1)$$

where  $P$  is the light power density and  $\alpha$  is the power exponent with an ideal value of 1, reflecting the linearity between photocurrent and light power density. As shown in Figure 3B, the fitted power exponent  $\alpha$  is 0.8, indicating the nearly linear photoresponse behavior of the prepared photodetector.

Responsivity ( $R$ ), a key parameter for photodetectors, represents the photocurrent that can be excited per unit

light power and can be calculated using the following equation:

$$R = \frac{I_{ph}}{P \cdot S} \quad (2)$$

where  $S$  is the effective illumination area. The calculated  $R$  values for different light power densities are plotted in Figure 3B.  $R$  increases monotonically with the decrease of light power density, and reach to the maximum value of 68 mA W<sup>-1</sup> at the light power density of 39 μW cm<sup>-2</sup>, which is higher than those of many reported GaN based self-powered UV photodetectors.<sup>44–47</sup> The external quantum efficiency (EQE) and specific detectivity ( $D^*$ ) are two other important figure of merits for photodetectors, which are defined by Equations (3) and (4)

$$EQE = \frac{R \cdot h \cdot c}{\lambda \cdot q} \quad (3)$$

$$D^* = R \cdot \sqrt{\frac{S}{2 \cdot q \cdot I_d}} \quad (4)$$

where  $h$  is the Planck constant,  $c$  is the velocity of light,  $\lambda$  is the wavelength, and  $I_d$  is the dark current. As shown in Figure 3C, both EQE and  $D^*$  increase with the

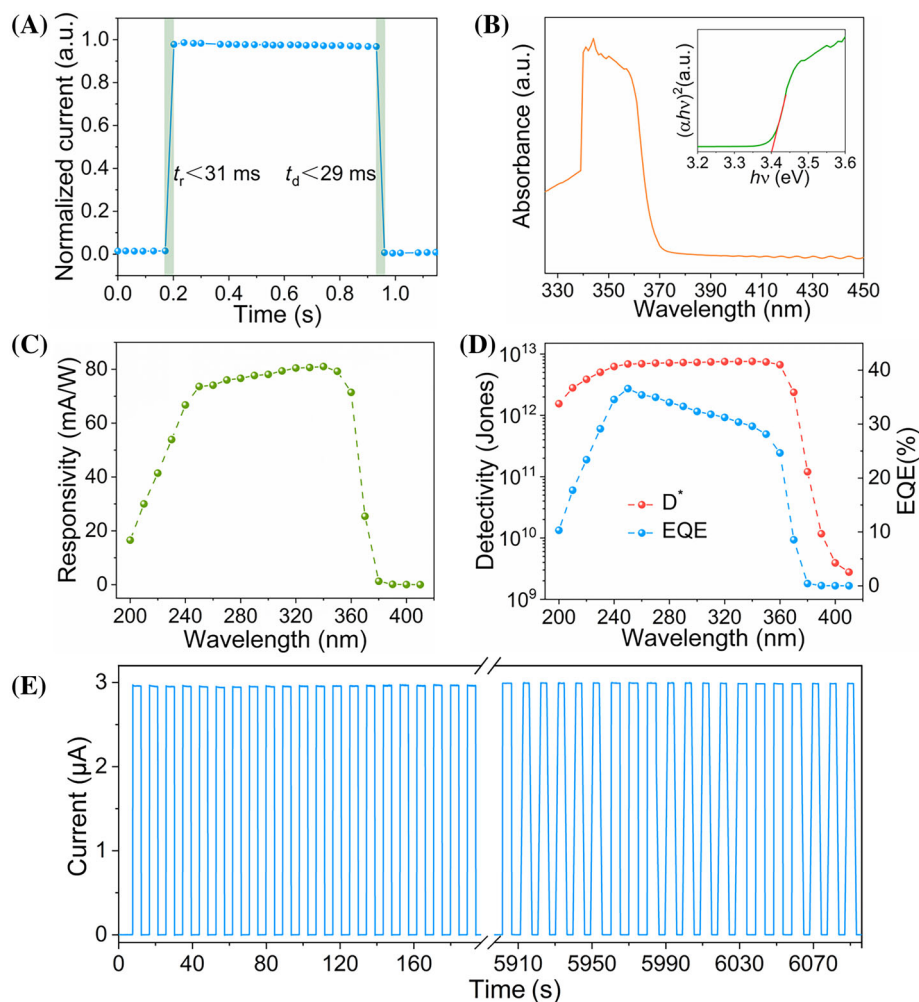


**FIGURE 4** (A) An enlarged switching cycle showing rise and decay times. (B) Absorbance spectra of the GaN film, inset is the calculated band gap of the GaN film. (C) Spectral responsivity and (D)  $D^*$ , EQE of the MXene/GaN photodetector at 0 V. (E) Cycle stability of the MXene/GaN photodetector.

decreasing of light power density, and the peak values are 23.5% and  $6.35 \times 10^{12}$  Jones, respectively.

The response speed of a photodetector, which is closely related to the transport and collection process of carriers, reflects its ability to track dynamic optical signals. The pulse response test results (Figure 4A) show that the rise time ( $t_r$ , defined as the time for the photocurrent to increase from 10% to 90%) and decay time ( $t_d$ , defined as the time for the photocurrent to decrease from 90% to 10%) of the photodetector are less than 31 and 29 ms, respectively. The obvious gap near rising and falling edge in Figure 4A indicates that the device has a faster response speed, but the sampling frequency of the test system is insufficient to support testing of the intrinsic response speed. The spectral response characteristics of the MXene/GaN photodetector were also investigated. Figure 4B shows the optical absorption spectrum of a GaN thick film. It can be observed that GaN has almost no absorption of visible light because of

its large bandgap; however, the absorbance increases sharply from 370 nm and drops after reaching a peak at 345 nm. The inset shows that the GaN bandgap calculated by *Tauc* plot from the absorption spectrum is 3.4 eV, which is consistent with the results reported in the literature.<sup>45</sup> Figure 4C shows the spectral responsivity (200–410 nm) of the MXene/GaN photodetector. The responsivity to incident light with wavelengths greater than 380 nm is extremely low, corresponding to the absorption spectrum of GaN and implying the prepared photodetector is visibly intrinsically blind. The peak responsivity of 81 mA W<sup>-1</sup> at 340 nm yield a high UV/visible rejection ratio ( $R_{340\text{nm}}/R_{400\text{nm}}$ ) of 1929. The wavelength-dependent EQE and  $D^*$  are plotted in Figure 4D, and they exhibit maximum values of 36.6% and  $7.57 \times 10^{12}$  Jones at 250 and 340 nm, respectively. The stability of a photodetector is crucial for practical applications, so we evaluated the stability of the MXene/GaN photodetector by cyclically switching it between the

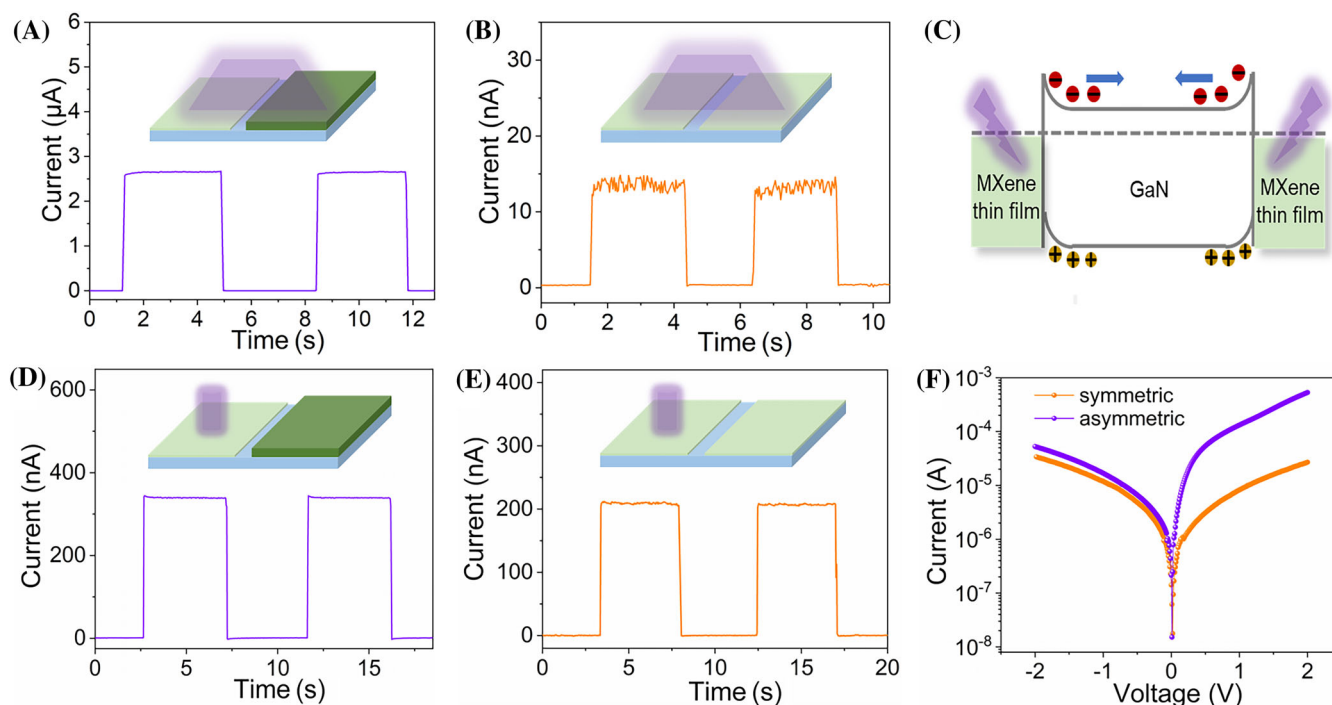


**FIGURE 5** Dynamic photoresponses of devices (A) with and (B) without the transmittance contrast of electrodes under the surface light source. (C) The band structure and carrier distribution of the corresponding device in (B) under the surface light source. Dynamic photoresponses of devices (D) with and (E) without the transmittance contrast of electrodes under the point light source. (F)  $I$ - $V$  curves of the corresponding devices in (D) and (E).

on and off state in air. As shown in Figure 4E, the photocurrent of the device did not fluctuate at all over 600 cycles, indicating its excellent cycle stability. In addition, the temporal stability of the device and the effect of MXene oxidation on the device performance were studied, as discussed in detail in Figures S10–S14. Compared with the reported GaN-based self-powered photodetectors, our device demonstrates outstanding comprehensive performance (see Table S1).

Considering that in the case of a point light source (laser), the illumination conditions in the two electrode regions are inherently asymmetric regardless of whether there is a contrast in the electrode transmittance, so we further investigated the photoelectric response under surface and point light sources. As shown in Figure 5A, the device with asymmetric transmittance of electrodes exhibits an obvious photoelectric response with a photocurrent up to 2.7  $\mu$ A under a surface light source. However, when both the MXene electrodes were transparent, the device exhibited almost no response, with a photocurrent of only 13 nA under the same light source (Figure 5B). This is due to the fact that the photocurrents generated in two Schottky junctions with the same MXene transparent electrodes are equal but opposite, resulting in a net current of zero, as shown in Figure 5C. This negligible photocurrent may have arisen from the

slight inhomogeneity of the transparent MXene electrode. The photocurrent increased with the electrode transmittance contrast (Figure S15). Under a point light source, the photocurrent of the device with symmetric MXene transparent electrodes increases significantly because the light received by the left and right Schottky junctions is inherently asymmetric (Figure 5E). However, the photoresponse of the device with an asymmetric transmittance of the electrodes is still obviously superior in this case, as shown in Figure 5D. This is because MXene thick film has a lower sheet resistance (Figure S13), and contact resistance with GaN (as indicated by the  $I$ - $V$  curves in Figure 5F), making it easier for laterally diffused electrons to tunnel from GaN into the MXene electrode. As expected, the device with two opaque electrodes of MXene thick films did not respond to any light source because the GaN in both Schottky junction regions could not receive light to generate photogenerated carriers (Figure S16). The device with contrasting transmittances of MXene electrodes has better performance under both light sources, which indicates that the designed photodetector can meet the practical application requirements under different forms of light sources, and also shows that constructing self-powered photodetectors through the asymmetric transmittance of electrodes is a preferred strategy. In addition, we surprisingly found that even

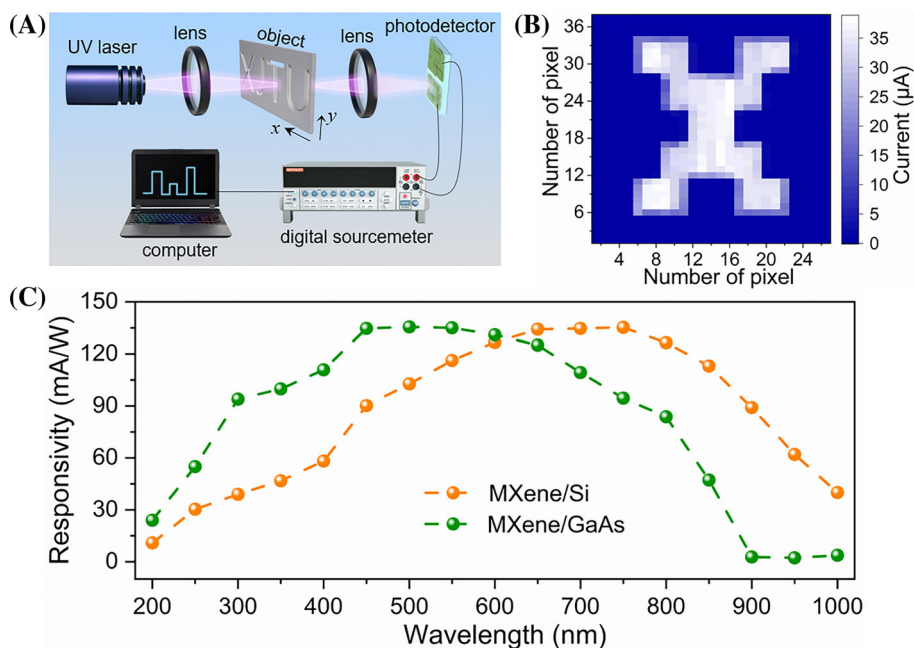


**FIGURE 6** (A) The schematic of the UV imaging system based on the MXene/GaN photodetector. (B) The pattern of letter “X” obtained from the UV imaging system. (C) Spectral responsivities of the MXene/Si and MXene/GaAs photodetectors.

though the two electrodes of MXene thin and thick films were connected, a considerable photocurrent could still be detected. Detailed tests and discussions are presented in Figure S17. This means that even if the two electrodes are accidentally connected during solution processing, they will not cause the device to short circuit and fail to work, demonstrating the excellent process latitude and flexibility of the proposed device structure.

High on/off ratio and good stability, which the MXene/GaN device just possesses, are necessary requirements for imaging application of photodetectors. Here, a UV imaging system was constructed to evaluate the imaging capability of the MXene/GaN photodetector. Figure 6A shows a schematic of the imaging system, in which a black acrylic plate with hollow letters is placed between the focused 360 nm laser and the MXene/GaN photodetector as a photomask. The photomask can be moved independently in two mutually perpendicular directions through a 2D translation stage controlled by a software-programmed stepper motor. The laser beam passing through the photomask excites the photodetector to generate a photocurrent. By mapping the photocurrent values to the 2D coordinates, an image of the hollow letters on the photomask can be obtained. Figure 6B shows the imaging result, in which a clear and well-resolved “X” letter pattern with 1026 ( $27 \times 38$ ) pixels is exhibited, indicating the good imaging capability of the MXene/GaN photodetector.

We further analyzed the superiority of MXene films as the transmittance modulators and carrier transport layer

over conventional metal electrodes. As shown in Figures S18A,B, the maximum responsivity of the Au/GaN device with a similar configuration is  $38.6 \text{ mA W}^{-1}$ , which is significantly lower than that of the MXene/GaN device. This is because the MXene thin film has a higher transmittance than the Au thin film while exhibiting a lower sheet resistance (Figure S18C,D). These results not only show that MXene film processed by a simple solution method are superior to vacuum-deposited Au film, but also demonstrate that the strategy of inducing a photocurrent through the contrast of electrode transmittance also works for metal/semiconductor structures. Furthermore, the designed device configuration should be applicable to any Schottky contact in an MXene/semiconductor structures. We have proved this by combining MXene with first- and second-generation semiconductors (Si and GaAs). As shown in Figure S19A,B, both the MXene/Si and MXene/GaAs devices exhibit obvious and stable optical switching behavior in the wavelength range determined by their bandgaps. The wavelength-dependent responsivities of each device calculated from Figure S19 were plotted in Figure 6C. The MXene/Si and MXene/GaAs photodetectors exhibit broadband responses (200–1000 nm) with peak responsivities of 135.3 and 135.5  $\text{mA W}^{-1}$ , respectively. These results conclusively demonstrate the universal applicability of the proposed strategy of inducing a photocurrent through transmittance contrast, and offer a disruptive technology for constructing self-powered photodetectors over a wide spectral range using MXene electrodes.



### 3 | CONCLUSION

In summary, we presented a general strategy for constructing self-powered photodetectors based on MXene/semiconductor Schottky junctions. The device was fabricated by depositing MXene electrodes with different transmittance on a semiconductor surface through all-solution processing. KPFM measurements indicated that the asymmetric carrier generation and injection between the two Schottky junctions resulting from the transmittance contrast induced a photocurrent at zero bias. The device with the transmittance contrast of the MXene electrodes exhibited a higher photoresponse than the device with all-transparent electrodes under both point and surface light sources. As an example, the MXene/GaN UV photodetector exhibits excellent performance, such as high responsivity ( $81 \text{ mA W}^{-1}$ ), fast response speed (less than 31 and 29 ms), ultrahigh on/off ratio ( $1.33 \times 10^6$ ) and good stability. In addition, it also shows good UV imaging capability as a single sensing pixel. The considerable responsivities of MXene/Si and MXene/GaAs self-powered photodetectors with similar configurations prove the universality of the proposed strategy for the first- to third-generation semiconductors. This work provides inspiration for the development of self-powered photodetectors based on a brand-new mechanism and demonstrates the promising applications of MXene in high-performance optoelectronic devices.

## 4 | EXPERIMENTAL SECTION

### 4.1 | Materials synthesis

The  $\text{Ti}_3\text{C}_2\text{T}_x$  colloidal solution was synthesized by selectively etching aluminum atoms from the purchased  $\text{Ti}_3\text{AlC}_2$  MAX powder (Jilin 11 Technology Co., Ltd.) followed by the ultrasonic treatment. Specifically, 2 g LiF was added to 20 mL concentrated hydrochloric acid in a Teflon beaker, and the mixture was stirred. Then, 1 g of  $\text{Ti}_3\text{AlC}_2$  MAX powder was slowly added to the above solution and stirred in an oil bath at  $40^\circ\text{C}$  for 24 h to completely etch the Al layers. After etching, the resulting product was washed repeatedly with deionized water by centrifugation (3500 rpm for 5 min) until almost neutral ( $\text{pH} \geq 6$ ). Deionized water was then added to the obtained wet sediment, and the mixture was ultrasonicated in an ice-water bath for 1 h. Finally, the product was centrifugated at 3500 rpm for 1 h, and the resulting supernatant, a dark green  $\text{Ti}_3\text{C}_2\text{T}_x$  colloidal solution, was collected.

### 4.2 | Device fabrication

The n-type GaN (Suzhou Nanowin Science and Technology Co., Ltd.), Si and GaAs (Hefei Kejing Material Technology Co., Ltd.) wafers were purchased from commercial sources. The fabrication process of different MXene/semiconductor devices are similar, so we use the MXene/GaN device as an example for a detailed description. The GaN wafer was sliced into  $1.5 \times 2 \text{ cm}^2$  pieces and ultrasonically washed with acetone, ethanol and deionized water in sequence. The cleaned GaN piece was further treated with air plasma to improve the surface hydrophilicity. A PVC electrostatic film with a width of 1 mm was attached to the middle of the GaN piece to isolate the two MXene electrodes of different thicknesses. The prepared  $\text{Ti}_3\text{C}_2\text{T}_x$  colloidal solution ( $5 \text{ mg mL}^{-1}$ ) was then spin-coated (2000 rpm for 15 s) onto the entire surface of GaN piece. Subsequently, the  $\text{Ti}_3\text{C}_2\text{T}_x$  colloidal solution was continuously drop-casted onto half of the surface of the sample obtained in the previous step, and the process was repeated after natural drying. Finally, the PVC film was peeled off and the resulting sample was heated in a  $\text{N}_2$  glovebox at  $120^\circ\text{C}$  for 10 min to enhance the contact between the MXene electrodes and GaN surface. Copper tapes were attached to the edges of the spin-coated and drop-casted MXene films, respectively for photoelectric measurements.

### 4.3 | Characterization and measurements

The phase structures of the samples were identified by XRD (Bruker D8 ADVANCE) with  $\text{Cu K}\alpha$  radiation. The transmittance and absorption spectra were collected using a spectrophotometer (Mapada V-1600PC). Raman spectrum was collected by a Raman spectroscopy (LabRAM HR Evolution) equipped with a 532 nm laser. The XPS and UPS spectra of MXene were tested through an x-ray photoelectron spectrometer (Thermo Fisher ESCALAB Xi+). The thickness test of MXene nanosheets and KPFM measurements were performed through AFM with Pt/Ir coated Si probe (Bruker, SCM-PIT-V2). For the in-situ KPFM tests, the surface potentials of MXene thin film and thick film on the surface of the GaN wafer were first tested without UV illumination. After the surface potential of half the area of the film was tested, UV illumination was applied, and the change in the surface potential of the remaining half of the film was recorded. The morphologies of the samples were observed using SEM (Zeiss Gemini500) and TEM (JEOL JEM-F200). The sheet resistances of the MXene and Au thin film were

measured using a four-point probe resistance tester (Kaivo, FP-001). All electrical measurements were carried out through a digital sourcemeter (Keithley 2410). A 360 nm laser (CNI, UV-F-360-80 mW) and a tunable monochromatic light source (Zolix, Omni-λbright) were used as point light sources, and a 365 nm ultraviolet LED lamp with adjustable divergence angle was used as surface light source. Light power was calibrated by an optical power meter (OPHIR photonics, Israel).

## ACKNOWLEDGMENTS

The authors thank Prof. Junling Wang for the fruitful discussion. This work was supported by the National Natural Science Foundation of China (No. 51902250). H. F. would like to thank the support from the Guangdong Provincial Key Laboratory Program (Grant No. 2021B1212040001). Hong Wang acknowledges support from the Shenzhen Science and Technology Program (No. KQTD20180411143514543) and Shenzhen DRC project [2018]1433. The Instrument Analysis Center of Xi'an Jiaotong University, the Shiyanjia lab ([www.shiyanjia.com](http://www.shiyanjia.com)), and Dr. Junjiang Tian are acknowledged for their assistance with the measurements.

## CONFLICT OF INTEREST STATEMENT

The authors declare no conflicts of interest.

## ORCID

Huajing Fang  <https://orcid.org/0000-0002-1939-3700>

Ziqing Li  <https://orcid.org/0000-0002-8126-2728>

Xiaosheng Fang  <https://orcid.org/0000-0003-3387-4532>

Hong Wang  <https://orcid.org/0000-0003-3791-786X>

## REFERENCES

- García de Arquer FP, Armin A, Meredith P, Sargent EH. Solution-processed semiconductors for next-generation photodetectors. *Nat Rev Mater*. 2017;2(3):16100.
- Wang B, Zhong S, Xu P, Zhang H. Booming development and present advances of two dimensional MXenes for photodetectors. *Chem Eng J*. 2021;403:126336.
- Cai S, Xu X, Yang W, Chen J, Fang X. Materials and designs for wearable photodetectors. *Adv Mater*. 2019;31(18):1808138.
- Su L, Yang W, Cai J, Chen H, Fang X. Self-powered ultraviolet photodetectors driven by built-in electric field. *Small*. 2017;13(45):1701687.
- Tian W, Wang Y, Chen L, Li L. Self-powered nanoscale photodetectors. *Small*. 2017;13(45):1701848.
- Qiao H, Huang Z, Ren X, et al. Self-powered photodetectors based on 2D materials. *Adv Opt Mater*. 2019;8(1):1900765.
- Wen Z, Fu J, Han L, et al. Toward self-powered photodetection enabled by triboelectric nanogenerators. *J Mater Chem C*. 2018;6(44):11893-11902.
- Chen HY, Liu KW, Chen X, et al. Realization of a self-powered ZnO MSM UV photodetector with high responsivity using an asymmetric pair of Au electrodes. *J Mater Chem C*. 2014;2(45):9689-9694.
- Wang S, Chen R, Ren Y, et al. Highly-rectifying graphene/GaN Schottky contact for self-powered UV photodetector. *IEEE Photonic Tech L*. 2021;33(4):213-216.
- Meng J, Li Z. Schottky-contacted nanowire sensors. *Adv Mater*. 2020;32(28):2000130.
- Song W, Liu Q, Chen J, et al. Interface engineering Ti<sub>3</sub>C<sub>2</sub> MXene/silicon self-powered photodetectors with high responsivity and detectivity for weak light applications. *Small*. 2021;17(23):2100439.
- Fang H, Zheng C, Wu L, et al. Solution-processed self-powered transparent ultraviolet photodetectors with ultrafast response speed for high-performance communication system. *Adv Funct Mater*. 2019;29(20):1809013.
- Dai M, Chen H, Wang F, et al. Ultrafast and sensitive self-powered photodetector featuring self-limited depletion region and fully depleted channel with van der Waals contacts. *ACS Nano*. 2020;14(7):9098-9106.
- Zhang M, Hu Y, Wang S, et al. A nanomesh electrode for self-driven perovskite photodetectors with tunable asymmetric Schottky junctions. *Nanoscale*. 2021;13(40):17147-17155.
- Zhou C, Raju S, Li B, Chan M, Chai Y, Yang CY. Self-driven metal-semiconductor-metal WSe<sub>2</sub> photodetector with asymmetric contact geometries. *Adv Funct Mater*. 2018;28(45):1802954.
- Ezhilmaran B, Patra A, Benny S, et al. Recent developments in the photodetector applications of Schottky diodes based on 2D materials. *J Mater Chem C*. 2021;9(19):6122-6150.
- Fang H, Lin Z, Wang X, et al. Infrared light gated MoS<sub>2</sub> field effect transistor. *Opt Express*. 2015;23(25):031908.
- Koppens FHL, Mueller T, Avouris P, Ferrari AC, Vitiello MS, Polini M. Photodetectors based on graphene, other two-dimensional materials and hybrid systems. *Nat Nanotechnol*. 2014;9(10):780-793.
- Chen Y, Wang Y, Wang Z, et al. Unipolar barrier photodetectors based on van der Waals heterostructures. *Nat Electron*. 2021;4(5):357-363.
- Yin L, Li Y, Yao X, et al. MXenes for solar cells. *Nano-Micro Lett*. 2021;13(1):78.
- VahidMohammadi A, Rosen J, Gogotsi Y. The world of two-dimensional carbides and nitrides (MXenes). *Science*. 2021;372(6547):abf1581.
- Yang Q, Wang Y, Li X, et al. Recent progress of MXene-based nanomaterials in flexible energy storage and electronic devices. *Energy Environ Mater*. 2018;1(4):183-195.
- Zhang YZ, Wang Y, Jiang Q, el-Demellawi JK, Kim H, Alshareef HN. MXene printing and patterned coating for device applications. *Adv Mater*. 2020;32(21):1908486.
- Luo L, Huang Y, Cheng K, et al. MXene-GaN van der Waals metal-semiconductor junctions for high performance multiple quantum well photodetectors. *Light-Sci Appl*. 2021;10(1):177.
- Ma H, Jia L, Lin Y, et al. A self-powered photoelectrochemical ultraviolet photodetector based on Ti<sub>3</sub>C<sub>2</sub>T<sub>x</sub>/TiO<sub>2</sub> in situ formed heterojunctions. *Nanotechnology*. 2021;33(7):075502.
- Xu H, Ren A, Wu J, Wang Z. Recent advances in 2D MXenes for photodetection. *Adv Funct Mater*. 2020;30(24):2000907.
- Kang Z, Ma Y, Tan X, et al. MXene-silicon van der Waals Heterostructures for high-speed self-driven photodetectors. *Adv Electron Mater*. 2017;3(9):1700165.
- Deng W, Huang H, Jin H, et al. All-sprayed-processable, large-area, and flexible perovskite/MXene-based photodetector

- arrays for photocommunication. *Adv Opt Mater.* 2019;7(6):1801521.
29. Ma H, Fang H, Liu Y, et al. Fully transparent ultraviolet photodetector with ultrahigh responsivity enhanced by MXene-induced photogating effect. *Adv Opt Mater.* 2023;11(12):2300393.
30. Song W, Chen J, Li Z, Fang X. Self-powered MXene/GaN van der Waals heterojunction ultraviolet photodiodes with superhigh efficiency and stable current outputs. *Adv Mater.* 2021;33(27):2101059.
31. Yang Y, Jeon J, Park JH, et al. Plasmonic transition metal carbide electrodes for high-performance InSe photodetectors. *ACS Nano.* 2019;13(8):8804-8810.
32. Sun Y, Liu Z, Ding Y, Chen Z. Flexible broadband photodetectors enabled by MXene/PbS quantum dots hybrid structure. *IEEE Electr Device Lett.* 2021;42(12):1814-1817.
33. Perumal Veeramalai C, Yang S, Zhi R, et al. Solution-processed, self-powered broadband  $\text{CH}_3\text{NH}_3\text{PbI}_3$  photodetectors driven by asymmetric electrodes. *Adv Opt Mater.* 2020;8(15):2000215.
34. Han J, Fang C, Yu M, Cao J, Huang K. A high-performance Schottky photodiode with asymmetric metal contacts constructed on 2D  $\text{Bi}_2\text{O}_2\text{Se}$ . *Adv Electron Mater.* 2022;8(7):2100987.
35. Liu J, Ren JC, Shen T, et al. Asymmetric Schottky contacts in van der Waals metal-semiconductor-metal structures based on two-dimensional Janus materials. *Research.* 2020;2020:6727524.
36. Guo F, Yang B, Yuan Y, et al. A nanocomposite ultraviolet photodetector based on interfacial trap-controlled charge injection. *Nat Nanotechnol.* 2012;7(12):798-802.
37. Zhang Y, Wang YC, Wang L, Zhu L, Wang ZL. Highly sensitive photoelectric detection and imaging enhanced by the pyro-phototronic effect based on a photoinduced dynamic Schottky effect in 4H-SiC. *Adv Mater.* 2022;34(35):2204363.
38. Sun Y, Jiang L, Wang Z, et al. Multiwavelength high-detectivity  $\text{MoS}_2$  photodetectors with Schottky contacts. *ACS Nano.* 2022;16(12):20272-20280.
39. Gao XD, Fei GT, Zhang Y, Zhang LD, Hu ZM. All-optical-input transistors: light-controlled enhancement of plasmon-induced photocurrent. *Adv Funct Mater.* 2018;28(40):1802288.
40. Lipatov A, Alhabe M, Lukatskaya MR, Boson A, Gogotsi Y, Sinitkii A. Effect of synthesis on quality, electronic properties and environmental stability of individual monolayer  $\text{Ti}_3\text{C}_2$  MXene flakes. *Adv Electron Mater.* 2016;2(12):1600255.
41. Naguib M, Kurtoglu M, Presser V, et al. Two-dimensional nanocrystals produced by exfoliation of  $\text{Ti}_3\text{AlC}_2$ . *Adv Mater.* 2011;23(37):4248-4253.
42. Kurra N, Ahmed B, Gogotsi Y, Alshareef HN. MXene-on-paper coplanar microsupercapacitors. *Adv Energy Mater.* 2016;6(24):1601372.
43. Wang Z, Kim H, Alshareef HN. Oxide thin-film electronics using all-MXene electrical contacts. *Adv Mater.* 2018;30(15):1706656.
44. Yi C, Chen Y, Kang Z, et al. MXene-GaN van der Waals heterostructures for high-speed self-driven photodetectors and light-emitting diodes. *Adv Electron Mater.* 2021;7(5):2000955.
45. Li P, Shi H, Chen K, et al. Construction of GaN/ $\text{Ga}_2\text{O}_3$  p-n junction for an extremely high responsivity self-powered UV photodetector. *J Mater Chem C.* 2017;5(40):10562-10570.
46. Peng M, Liu Y, Yu A, et al. Flexible self-powered GaN ultraviolet photoswitch with piezo-phototronic effect enhanced on/off ratio. *ACS Nano.* 2015;10(1):1572-1579.
47. Yu N, Li H, Qi Y. NiO nanosheet/GaN heterojunction self-powered ultraviolet photodetector grown by a solution method. *Opt Mater Express.* 2018;9(1):26-34.

## SUPPORTING INFORMATION

Additional supporting information can be found online in the Supporting Information section at the end of this article.

**How to cite this article:** Ma H, Fang H, Li J, Li Z, Fang X, Wang H. Transmittance contrast-induced photocurrent: A general strategy for self-powered photodetectors based on MXene electrodes. *InfoMat.* 2024;6(5):e12540. doi:[10.1002/inf2.12540](https://doi.org/10.1002/inf2.12540)